

## Article

# Continuous Zonal Gradients Characterize Epipelagic Plankton Assemblages and Hydrography in the Subtropical North Atlantic

Antonio Bode , María Ángeles Louro, Elena Rey and Angel F. Lamas

Centro Oceanográfico de A Coruña, Instituto Español de Oceanografía, IEO-CSIC, 15001 A Coruña, Spain; gelines.louro@ieo.csic.es (M.Á.L.); elena.rey@ieo.csic.es (E.R.); a.lamas@ieo.csic.es (A.F.L.)

\* Correspondence: antonio.bode@ieo.csic.es; Tel.: +34-981218151

**Abstract:** The subtropical North Atlantic is a key region for understanding climate impact in the ocean. Plankton studies in this region have been generally framed in biogeographic provinces or focused on latitudinal gradients. In this study, we demonstrate the benefits of using empirically constructed continuous gradients versus the use of average values for biogeographical provinces to characterize plankton assemblages along a longitudinal transect at 24.5° N using an unprecedented array of stations including hydrographic observations, abundance of phytoplankton and zooplankton, and plankton size spectra in the epipelagic layer (0–200 m). In addition, the variability of zooplankton assemblages was analyzed using detailed taxonomic identification at selected stations. We found significant gradients in most hydrographic and plankton variables. The former, including surface temperature and salinity, the depth of the upper mixing layer, and the depth of the chlorophyll maximum, displayed non-linear gradients with maximum or minimum values near the center of the transect. In contrast, most plankton variables showed linear zonal gradients. Phytoplankton, microzooplankton (<100 µm), and the slope and the intercept of the size spectra increased (and *Trichodesmium* decreased) to the west. Total mesozooplankton (>200 µm) did not show any significant zonal pattern, but the taxonomic assemblages were characterized by a gradual replacement of large Calanoids by small-bodied Cyclopoid copepods from east to west. The use of continuous gradients provides more detailed information on the zonal structure of subtropical plankton than the classical approach using discrete areas.

**Keywords:** phytoplankton; zooplankton; size spectra; taxonomic composition; subtropical ocean



**Citation:** Bode, A.; Louro, M.Á.; Rey, E.; Lamas, A.F. Continuous Zonal Gradients Characterize Epipelagic Plankton Assemblages and Hydrography in the Subtropical North Atlantic. *Oceans* **2024**, *5*, 109–126. <https://doi.org/10.3390/oceans5010007>

Academic Editor: Antonella Penna

Received: 10 October 2023

Revised: 5 February 2024

Accepted: 27 February 2024

Published: 1 March 2024



**Copyright:** © 2024 by the authors. Licensee MDPI, Basel, Switzerland. This article is an open access article distributed under the terms and conditions of the Creative Commons Attribution (CC BY) license (<https://creativecommons.org/licenses/by/4.0/>).

## 1. Introduction

The subtropical ocean is expected to receive one of the largest impacts from climate change [1]. Particularly in the North Atlantic, the variability in the properties of subtropical waters has profound implications for climate change, showing decadal warming [2,3], slowdown of the Atlantic Meridional Overturning Circulation (AMOC [4]), and increasing oligotrophy [5–7], among other changes recently reported. Plankton communities in subtropical waters can be highly sensitive to climate changes because they are characterized by low abundance and biomass, dominance of small organisms [8,9], low primary production rates [5] but significant N fixation by cyanobacteria [10,11], predominance of microbial food webs [9], and food chains longer than those found in productive waters [12].

The subtropical gyres of the North Atlantic have a major influence in the circulation and retention of surface waters constraining two major biogeographical domains. These are identified as the North Atlantic Subtropical East (NASE) and North Atlantic Subtropical West (NASW) biogeographic provinces [13], or as the Winter Subtropical (WIS) and Summer Subtropical (SUS) phytoplankton biomes [14]. Average properties (hydrography, nutrient supply, plankton composition) of these regions have been used for descriptive and modelling purposes [14,15]. For instance, the distinction between NASE and NASW

is justified by the presence of the Mid-Atlantic Ridge, as both are weakly influenced by the westerly winds and are part of the same anticyclonic subtropical gyre, but also by the relatively restricted circulation of the Sargasso Sea (NASW) and by the shoaler mixed-layer depths offshore the Canary Current (NASE). Both provinces are characterized by seasonal cycles of thermal stratification and winter mixing, with phytoplankton blooms related to the advection of deep nutrients in spring but also to eddies and upwelling filaments, particularly in NASE. However, these regions show relatively large zonal differences (i.e., along the geographic longitude gradient) in hydrography [2–4], acidification [16,17], and plankton [18–22]. Detailed studies for this region concentrating on physical oceanography properties systematically observed it along zonal transects in the framework of international programs, such as the World Ocean Circulation Experiment (WOCE). For instance, the repeated standard section A05 at 24.5° N provided key observations for understanding recent and past changes in circulation and heat fluxes [2–4,23]. In contrast, studies of plankton and biogeochemical fluxes were generally made using observations collected on a variety of longitude and latitude positions in this region. For instance, a dome-shaped distribution was reported for some variables relevant for the regional biogeochemistry, such as the depth of the thermocline and the chlorophyll maximum [21,24] or the importance of nitrogen fixation and diazotrophic organisms [19,22,25]. However, small zonal variation was reported for other properties such as bacterial biomass, primary production, and community respiration [24], or for the plankton size structure [21]. Seasonal variability is relatively small in this region, but may partly explain these differences [20,24].

While the current observations of plankton properties in the subtropical North Atlantic fit in general within the framework of discrete biogeographic provinces, the relatively large variability within each province suggests the participation of other factors besides those caused by gyre circulation. A quantitative description of the zonal variability of the plankton assemblages in the subtropical North Atlantic gyres, as an alternative to a discrete province-based approach, has never been attempted.

The objective of this study is to demonstrate the benefits of using empirically constructed continuous gradients versus the use of average values for discrete biogeographical domains to describe the variability in plankton composition and size structure in the form of continuous gradients along a zonal transect in the epipelagic layer (0–200 m depth) of the North Atlantic. We present, for the first time, detailed observations on abundance, biomass, and size distributions of phytoplankton (including colonies of the nitrogen-fixer *Trichodesmium*), microzooplankton (40–100 µm), and mesozooplankton (200–2000 µm) collected on the WOCE standard section at 24° N. Besides, we report the taxonomic composition of mesozooplankton assemblages. The results will be applicable to future studies aiming to predict the impacts of climate change on this region.

## 2. Materials and Methods

### 2.1. Sampling and Hydrographic Observations

Sampling was made between January and March 2011 on R/V Sarmiento de Gamboa during leg 8 of the Malaspina 2010 Expedition (<http://www.expedicionmalaspina.es>, accessed on 1 March 2024). We made detailed CTD profiles between the surface and ca. 5000 m on 167 stations with a CTD-rosette system equipped with conductivity, salinity, depth, and chlorophyll fluorescence sensors. For this study, a subset of 43 stations were selected for plankton sampling by vertical tows of nets through the upper 200 m of the water column between 10:00 and 16:00 h UTC (Figure 1). Dissolved oxygen and inorganic nutrient concentrations were determined in water samples collected from the rosette bottles at standard depths. In this study, we employ average concentrations determined from 3 to 5 individual samples from the upper mixing layer for each station. Dissolved oxygen was determined by Winkler titration and total nitrate (nitrate plus nitrite), total reactive silica, and phosphate by colorimetric methods [26]. From the CTD profiles, sea surface temperature (SST) and salinity (SSS), along with the depth of the upper mixing layer (MLD) and the depth of the chlorophyll maximum (DCM), were retained for this study. MLD

was estimated using the threshold method [27] as the depth where the difference between the in situ density and that of the surface exceeded  $0.125 \text{ kg m}^{-3}$ . Hydrographic data for this cruise can be found in the database of CLIVAR and Carbon Hydrographic Data Office (CCHDO) [28]. In addition, chlorophyll fluorescence (measured in relative units) was used as a proxy of phytoplankton biomass for the upper mixing layer. Phytoplankton and microzooplankton were collected between the surface and 200 m depth by vertical tows of a net of 30 cm diameter equipped with  $40 \mu\text{m}$  mesh, while mesoplankton was sampled similarly by using a 50 cm diameter net equipped with a  $200 \mu\text{m}$  mesh. Phytoplankton and microzooplankton samples were preserved in glutaraldehyde (25% final concentration), and mesozooplankton samples were preserved in formalin (4% final concentration) for later analysis in the laboratory. Additional observations from the same cruise were reported in previous studies [19,22,23,29].

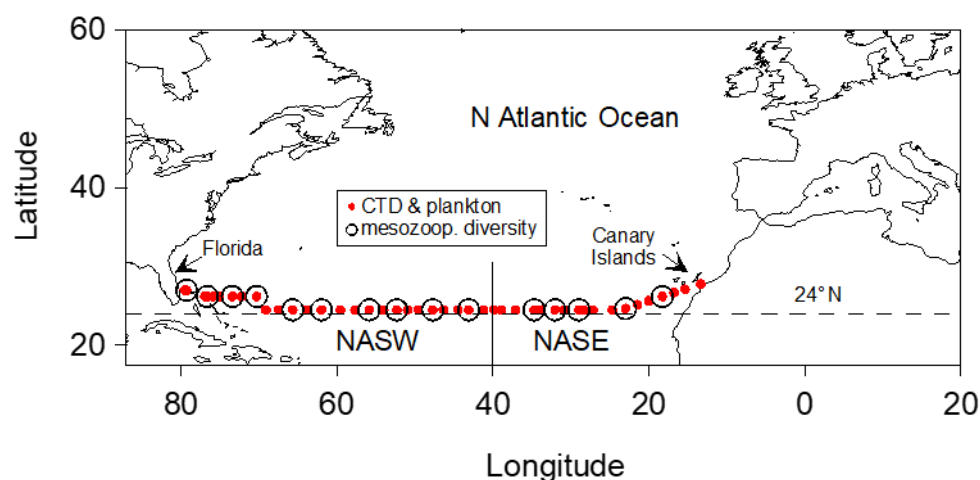


**Figure 1.** Position of sampled stations along the subtropical North Atlantic. The biogeographic provinces North Atlantic Subtropical West (NASW) and North Atlantic Subtropical East (NASE) are indicated. The stations where detailed mesozooplankton taxonomic composition was studied are encircled (mesozoop. diversity).

## 2.2. Plankton Abundance, Individual Size, and Composition

Phytoplankton and microplankton abundance and size were determined using a semiautomatic image analysis flow-through system (FlowCAM) [30]. A subsample was first screened through a  $100 \mu\text{m}$  mesh to exclude large particles and then introduced in a 100 mm diameter flow cell. Particles were photographed in auto-image mode using an objective of  $\times 10$  (total magnification  $\times 100$ ). Images were classified using VisualSpreadsheet Particle Analysis Software (version 3.2, Fluid Imaging Technologies Inc., Yarmouth, MA, USA) for FlowCAM [31] and user validated in the following categories: phytoplankton (including diatoms and dinoflagellates), *Trichodesmium*, and microzooplankton. Detritus and other particles not clearly attributable to living organisms were excluded from the final counts. Size of plankton was determined from the surface ( $\text{mm}^2$ ) of individual images using the “(Area (ABD))” variable determined by VisualSpreadsheet. Surface was later converted to carbon biomass using an empirical equation determined for this cruise (Figure 2) using the data on particulate organic carbon (POC) measured in size-fractionated plankton samples, and determined using elemental analysis [19].

Mesozooplankton abundance was determined in all samples using a scanning analysis system (ZooImage, <https://www.sciviews.org/zooimage/>, accessed on 2 November 2016) [32]. Three subsamples, including at least 300 individual zooplankters, were scanned for each sample at 1200 dpi ( $21 \mu\text{m}$  per pixel) using an EPSON 1640 flat scanner (Epson Europe Electronics GmbH, München, Germany) and microtiter polystyrene plates (Corning Inc., Corning, NY, USA). The resulting images were analyzed with the ZooImage software (version 1.2-0) to obtain the total number of organisms and the surface of each individual image

(“Area ROI” in ZooImage, mm<sup>2</sup>). Individual surface was later converted in to carbon biomass as for FlowCAM images. In addition, taxonomic composition of zooplankton was determined using microscope examinations of selected samples. Species were identified for Copepoda, Branchiopoda, and Ostracoda, while other groups were classified at higher taxonomic level. Scientific names were assigned following the World Register of Marine Species (WoRMS) [33]. *Trichodesmium* abundance data can be found in Version 2 of the Global Oceanic Diazotroph Database [34].

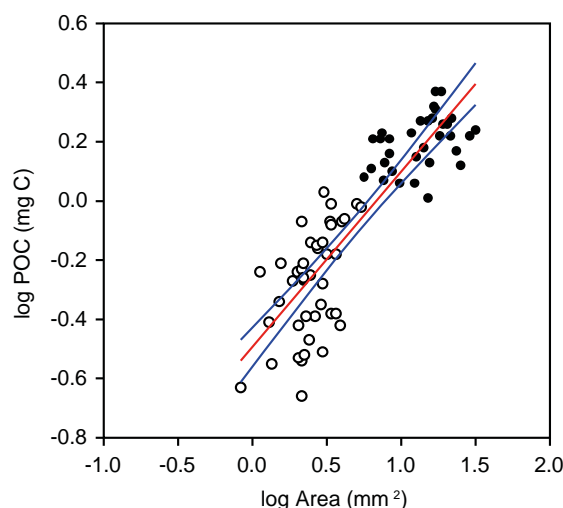


**Figure 2.** Log-log regression between particulate organic carbon (POC, mg C) and total area of particles (mm<sup>2</sup>) determined using FlowCAM (open dots) and ZooImage (filled dots) per m<sup>3</sup> in the sampled plankton stations. The regression line (red) and 95% confidence limits (blue) are indicated ( $r = 0.866$ ,  $p < 0.001$ ). The regression slope ( $0.593 \pm 0.040$  mg C mm<sup>-2</sup>) was used to estimate the carbon biomass of particles from their area. Circles and are indicated in the legend as “open dots” and “filled dots”, respectively.

### 2.3. Abundance Size Spectra

Plankton size distributions were summarized as biomass-normalized abundance spectra [35,36]. These spectra were computed from the abundance and individual biomass determined from image analysis values for each sample using equations in the form:

$$\log_2 (B_i / w_i) = \text{NBSI} + \text{NBSS} \log_2 w_i \quad (1)$$

where  $B_i$  and  $w_i$  are the abundance and carbon biomass of classes of doubling size, respectively. Each size distribution is thus characterized by the intercept (NASI) and slope (NASS) of the biomass-normalized abundance spectrum. A total of 15 logarithmic size classes spanning an individual biomass range between 0.125 and 512  $\mu\text{g C}$  were obtained by combining FlowCAM and ZooImage counts (Figure 3).

### 2.4. Statistical Analyses

Differences in mean values of individual variables between NASW and NASE provinces were assessed with Student *t*-tests (critical significance value  $p = 0.05$ ). Zonal distribution of hydrographic and plankton variables was quantified using Ordinary Least Squares (OLS) regression with geographic longitude as the independent variable. Linear fits were first assayed, but 2nd. degree polynomial fits were retained when it caused an increase in the value of the determination coefficient ( $r^2$ ) or a decrease in the value of the Akaike Information Criterion (AIC). Significance of the regression lines was assessed by an F test, and 95% confidence limits for the regression were estimated by the Working-Hotelling procedure [37].

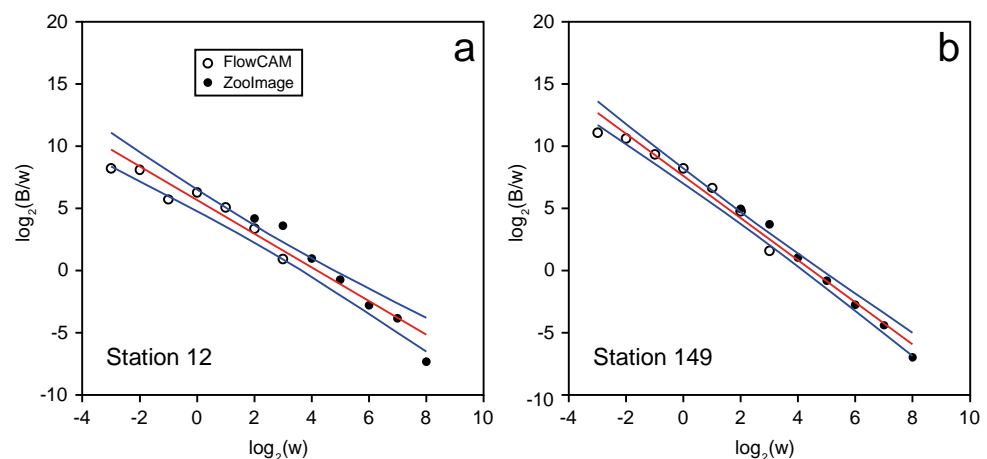


**Figure 3.** Examples of biomass-normalized size spectra by combining counts obtained with the FlowCAM (open dots) and ZooImage (filled dots) for (a) Station 12 (eastern end of the transect) and (b) Station 149 (western end of the transect). The spectra are indicated by the regression lines (red) and 95% confidence limits (blue).  $w$ : nominal size of each size class ( $\mu\text{g C}$ ),  $B$ : biomass ( $\mu\text{g C m}^{-3}$ ).

Ordination of mesozooplankton taxonomic data was made using Multidimensional Scaling (MDS) using the Morisita distance for abundance data [38]. The original abundance data were rearranged to ensure that all taxa employed in the analysis were present in at least 25% of samples. The two first MDS axis were regressed against longitude. The grouping of stations was further supported by cluster analysis constrained to the NASE and NASW provinces using the Morisita similarity index and the unweighted pair-group average method. Finally, an overall ordination of samples was made using Principal Component Analysis (PCA) on geographical longitude (Lon), hydrographic (SST, SSS, MLD, DCM), and plankton variables (NBSS, NBSI, and abundance of *Trichodesmium*, microzooplankton, and mesozooplankton). The two first components were also regressed against geographical longitude. All statistical analyses were run using PAST v 4.09 [39].

### 3. Results

#### 3.1. Hydrography

Mean values of most hydrographic variables considered (except mean nitrate concentrations and DCM) showed significant differences between NASE and NASW provinces (Table 1). For instance, NASE had lower SST but higher SSS, MLD, fluorescence, oxygen, silicate, and phosphate concentrations in the upper mixed layer than NASW. Most variables were significantly correlated with SSS, SST, DCM, or MLD (Supplementary Table S1). However, these variables also showed non-linear zonal patterns (Figure 4). Temperature at the surface was near  $21\text{ }^{\circ}\text{C}$  in the east, but progressively increased towards the western end of the transect, where it showed the largest variability. Conversely, SSS, MLD, and DCM decreased in general to the west, but reached maximum values (SSS ca. 37.5) near  $40^{\circ}\text{ W}$ , the boundary between NASE and NASW provinces. All these zonal patterns were described by 2nd order polynomial functions (Supplementary Table S2).

#### 3.2. Plankton Size-Spectra and Abundance

All plankton size distributions were significantly fitted to log-linear normalized size-spectra, with slope values between  $-2.04$  and  $-1.15$  (Supplementary Table S3). The zonal variation of the plankton size-spectra followed a lineal pattern (Figure 5, Supplementary Table S4), with mean values of the intercept (but not of the slope) significantly higher in NASW (Table 1). The slope values decreased from east to west, while the intercepts showed an opposite pattern. In this case, there was no sharp change in the zonal pattern near the boundary between NASE and NASW.

**Table 1.** Mean ( $\pm$ SD) values for the variables considered in this study for NASE and NASW provinces. SST, SSS, and SFluor: surface temperature ( $^{\circ}$ C), salinity, and fluorescence (relative units), respectively; DCM: depth of the chlorophyll maximum (m); MLD: mixed layer depth (m); MLO<sub>2</sub>, MLNO<sub>3</sub>, MLSiO<sub>2</sub>, MLPO<sub>4</sub>, and MLFluor: mixed layer dissolved oxygen (ml L<sup>-1</sup>), nitrate ( $\mu$ M), silicate ( $\mu$ M), phosphate ( $\mu$ M), and fluorescence (relative units), respectively; MNBSS and NBSI: slope and intercept of the biomass-normalized spectrum, respectively; Tricho, phyto, microz, mesoz, Cope, Tunic, Cnid, and Other: abundance of *Trichodesmium* (trichomes L<sup>-1</sup>), phytoplankton (cells L<sup>-1</sup>), microzooplankton (indiv. L<sup>-1</sup>), mesozooplankton (indiv. m<sup>-3</sup>), Copepoda (indiv. m<sup>-3</sup>), Tunicata (indiv. m<sup>-3</sup>), Cnidaria (indiv. m<sup>-3</sup>), and other mesozooplankton taxa (indiv. m<sup>-3</sup>), respectively. Number of data are indicated between parenthesis. *p*: significance of means (Student-*t* test, *p* < 0.05 values are indicated in boldface).

Variable	NASW	NASE	<i>p</i>
	Mean $\pm$ SD (n)	Mean $\pm$ SD (n)	
SST	23.63 $\pm$ 0.76 (25)	22.13 $\pm$ 0.76 (17)	<b>0.000</b>
SSS	36.86 $\pm$ 0.38 (25)	37.28 $\pm$ 0.24 (17)	<b>0.000</b>
SFluor	0.11 $\pm$ 0.04 (25)	0.20 $\pm$ 0.13 (17)	<b>0.014</b>
DCM	113.88 $\pm$ 22.76 (25)	115.71 $\pm$ 27.52 (17)	0.816
MLD	75.72 $\pm$ 25.25 (25)	97.12 $\pm$ 27.78 (17)	<b>0.013</b>
MLO <sub>2</sub>	4.83 $\pm$ 0.07 (24)	4.89 $\pm$ 0.08 (17)	<b>0.029</b>
MLNO <sub>3</sub>	0.13 $\pm$ 0.08 (17)	0.21 $\pm$ 0.22 (16)	0.178
MLSiO <sub>2</sub>	0.30 $\pm$ 0.33 (17)	0.73 $\pm$ 0.17 (16)	<b>0.000</b>
MLPO <sub>4</sub>	0.35 $\pm$ 0.27 (17)	0.57 $\pm$ 0.14 (16)	<b>0.007</b>
MLFluor	0.13 $\pm$ 0.05 (25)	0.20 $\pm$ 0.09 (17)	<b>0.003</b>
NBSS	-2.71 $\pm$ 0.12 (25)	-2.62 $\pm$ 0.17 (17)	0.066
NBSI	6.53 $\pm$ 0.55 (25)	6.10 $\pm$ 0.67 (17)	<b>0.025</b>
Tricho	59.84 $\pm$ 46.56 (25)	81.00 $\pm$ 83.69 (17)	0.300
phyto	128.38 $\pm$ 70.48 (26)	74.37 $\pm$ 29.37 (17)	<b>0.001</b>
microz	185.92 $\pm$ 73.83 (26)	147.95 $\pm$ 121.24 (17)	0.208
mesoz	156.46 $\pm$ 93.45 (25)	178.04 $\pm$ 133.63 (17)	0.541
Cope	175.34 $\pm$ 187.66 (9)	112.82 $\pm$ 132.09 (6)	0.494
Tuni	35.50 $\pm$ 35.07 (9)	23.57 $\pm$ 23.74 (6)	0.481
Cnid	4.43 $\pm$ 3.18 (9)	5.53 $\pm$ 5.87 (6)	0.644
Other	29.56 $\pm$ 22.23 (9)	23.28 $\pm$ 31.62 (6)	0.657

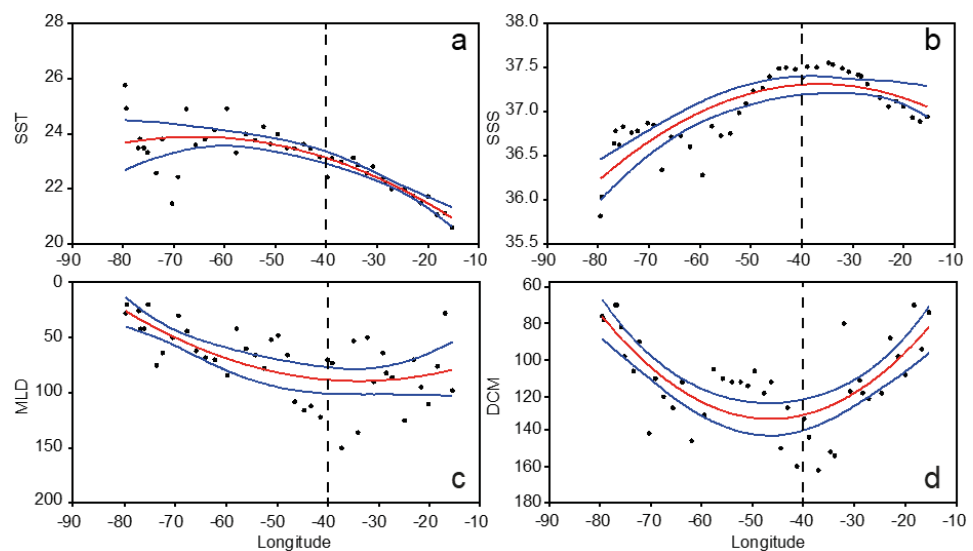


**Figure 4.** Variation with the geographical longitude (degrees, negative to the west) of (a) sea surface temperature (SST,  $^{\circ}$ C), (b) sea surface salinity (SSS), (c) the depth of the upper mixing layer (MLD, m), and (d) the depth of the chlorophyll maximum (DCM, m). The patterns are indicated by 2nd degree polynomial regression lines (red) and 95% confidence limits (blue). Parameters of the regressions are listed in Supplementary Table S2. The limits between NASE and NASW are indicated by the vertical dashed lines. Note that the Y-axes are inverted for panels (c,d).

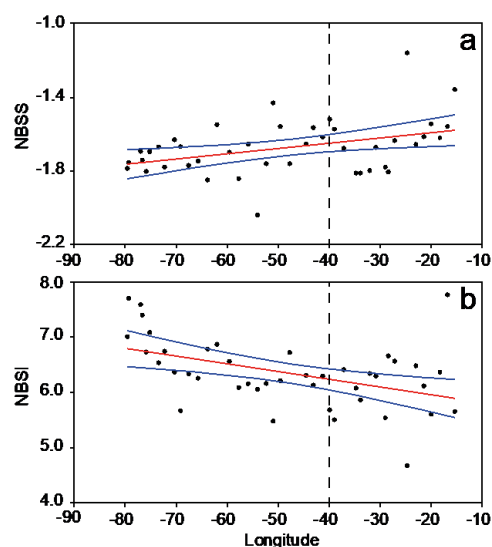


**Figure 5.** Variation with the geographical longitude (degrees, negative to the West) of the biomass-normalized abundance plankton spectra: (a) slope (NBSS,  $\log_2 [\text{m}^{-3} \mu\text{g C}^{-1}]$ ); (b) intercept (NBSI,  $\log_2 [\text{m}^{-3}]$ ). The patterns are indicated by linear regression lines (red) and 95% confidence limits (blue). Parameters of the regressions are listed in Supplementary Table S4. The limits between NASE and NASW are indicated by the vertical dashed lines.

Phytoplankton and microplankton abundance increased linearly to the west as the spectral slope, but *Trichodesmium* and mesozooplankton had different patterns (Figure 6, Supplementary Table S4). Abundance of *Trichodesmium* was very low ( $<10$  trichomes  $\text{L}^{-1}$ ) between 15 and 25° W, but reached maximum values near 30° W ( $>300$  trichomes  $\text{L}^{-1}$ ) and decreased linearly towards the west, where it was still detectable (10–40 trichomes  $\text{L}^{-1}$ ). Mesozooplankton, however, did not display any clear zonal pattern, with generally low abundance values through the transect ( $<200$  indiv.  $\text{m}^{-3}$ ) but with some increases in variability at both ends of the transect. Similarly, no significant zonal pattern could be identified when considering separately taxonomic groups as Copepoda, Tunicata, Cnidaria, and other groups (Supplementary Table S4). Only mean phytoplankton abundance was significantly higher in NASW (Table 1).

### 3.3. Mesozooplankton Taxonomic Assemblages

A total of 127 mesozooplanktonic taxa were identified, including 75 species of Copepoda, 3 species of Branchiopoda, and other groups at lower taxonomic resolution (Supplementary Table S5). Copepods generally dominated, followed by tunicates (i.e., Appendicularia, Doliolida, and Salpida), and other groups. The detailed classification was rearranged, and 65 taxa were used for the MDS. The ordination in the two first axes (stress = 0.143) allowed for a separation of stations following the biogeochemical provinces (Figure 7). This separation was further confirmed by the cluster analysis (Supplementary Figure S1). However, while there was no clear zonal pattern for the scores of the first MDS axis, there was a significant lineal increase of the scores of the second MDS axis to the west. Samples from stations located in the NASE province had mostly negative scores in the second MDS axis. The first MDS axis (Table 2) was positively correlated with the abundance of several species of Calanoid Copepoda (including *Calanus helgolandicus*, *Microcalanus pygmaeus*, *Phaenna spinifera*, *Undinula vulgaris*, and species of *Subeucalanus*, *Eucalanus*, *Rhincalanus*, and *Calocalanus*), but also with some small ( $<1$  mm) Cyclopoid Copepoda (*Oncaea*) and Ostracoda (*Conchoecia*). Negative correlations of this axis were found with other Calanoid Copepoda (*Mesocalanus tenuicornis*, *Paracalanus* spp.), Decapoda larvae and Euphausiacea, and large sized ( $>1.5$  mm) Cyclopoid Copepoda (*Lubbockia* spp.). The second MDS axis was positively correlated with the abundance of small sized (0.5–1.5 mm) Cyclopoid Copepoda (*Oithona* spp.) and Foraminifera, but also with medium-sized (1.5 mm)

Calanoid Copepoda (*Haloptilus* spp.). The second axis showed negative correlations with medium and large sized (1–2.5 mm) Calanoid Copepoda (*Haloptilus longicornis*, *Acartia* spp.), but also with small sized (<1 mm) Cyclopoid Copepoda (*Oncaea*).

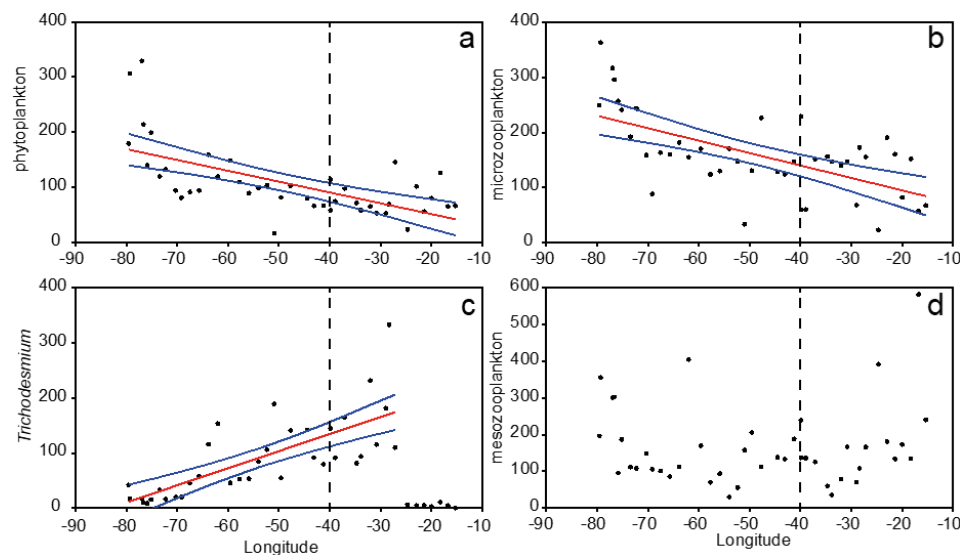


**Figure 6.** Variation with the geographical longitude (degrees, negative to the west) of (a) phytoplankton (indiv.  $L^{-1}$ ), (b) microzooplankton (indiv.  $L^{-1}$ ), (c) *Trichodesmium* (trichomes  $L^{-1}$ ), and (d) mesozooplankton (indiv.  $m^{-3}$ ). The patterns are indicated by lineal regression lines (red) and 95% confidence limits (blue). Parameters of the regressions are listed in Supplementary Table S4. The limits between NASE and NASW are indicated by the vertical dashed lines.

### 3.4. Overall Zonal Patterns

The geographical longitude of the stations was significantly correlated with most hydrographic and plankton variables (Table 3). The notable exceptions were *Trichodesmium* and mesozooplankton abundances. *Trichodesmium*, however, was significantly correlated with longitude only when stations east of  $25^{\circ}$  W were excluded (Figure 6c). As a consequence, the correlation between hydrographic and plankton variables reflected their relationships with longitude. For instance, SST was positively correlated with NBSI and with phytoplankton and microzooplankton abundance, while it displayed negative correlations with SSS, surface chlorophyll fluorescence, and NASS. Similarly, SSS showed positive correlations with DCM and MLD, and negative correlations with plankton variables that were positively correlated with SST. Among the variables that did not show significant correlations with longitude, surface chlorophyll fluorescence only showed significant negative correlations with SST and DCM, the latter showing non-linear variation with longitude (Figure 4d). In contrast, the spectral parameters showed linear zonal patterns and were either positively correlated with MLD and mesozooplankton (NASS), or with SST and most plankton groups (NASI), and negatively correlated with SST, NASI, phytoplankton, and microzooplankton (NASS). *Trichodesmium* abundance was positively correlated with SSS and DCM, and negatively with the abundance phytoplankton and Cnidaria. Phytoplankton and microzooplankton were significantly correlated and displayed positive correlations with SST, NASI, and most other groups of plankton, except with total mesozooplankton, and microzooplankton with *Trichodesmium* and Cnidaria. Mesozooplankton abundance was only positively correlated with the spectral parameters, while the abundances of the selected taxonomic groups were mostly correlated between them, but also with phytoplankton and NASI.

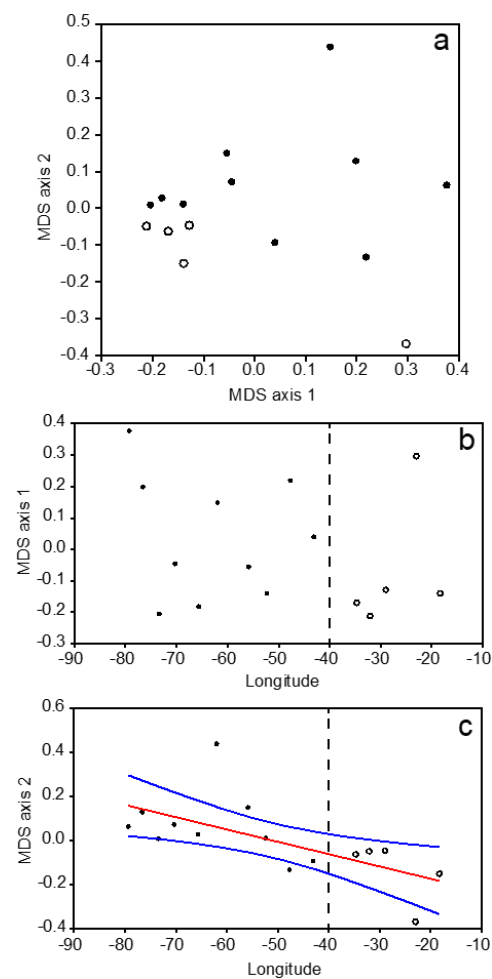


**Figure 7.** Non-metric Multidimensional Scaling (MDS) of mesozooplankton community samples (stress = 0.143). (a) Projection of samples in the two first axes and variation with the geographical longitude (degrees, negative to the west) of (b) the scores on the first and (c) second axis. The significant regression line (red) and 95% confidence limits (blue) are indicated. Samples from the Longhurst provinces NASE and NASW are indicated by open and filled dots, respectively. Circles and dots are explained in the caption as “open dots” and “filled dots”, respectively.

**Table 2.** Scores of the main mesozooplankton species or groups with the two first axes of the non-metric multidimensional scaling (MDS1 and MDS2, respectively) on the mesozooplankton community samples.

Species/Group	MDS 1	Species/Group	MDS 2
Calanoida (other)	0.911	<i>Oithona plumifera</i>	0.533
<i>Oncaea</i> spp.	0.495	<i>Oithona</i> spp.	0.220
<i>Conchoecia</i> spp.	0.484	Foraminifera	0.176
<i>Lucicutia</i> spp.	0.317	<i>Haloptilus</i> sp.	0.099
<i>Calocalanus</i> spp.	0.207	<i>Lubbockia</i> sp.	0.091
<i>Lubbockia</i> sp.	-0.154	<i>Acartia negligens</i>	-0.105
Euphausiacea	-0.170	<i>Oncaea</i> spp.	-0.158
Decapoda (larvae)	-0.278	<i>Acartia</i> spp.	-0.225
<i>Paracalanus</i> spp.	-0.356	Calanoida (other)	-0.298
<i>Mesocalanus tenuicornis</i>	-0.453	<i>Haloptilus longicornis</i>	-0.302

**Table 3.** Values of the Pearson correlation coefficients (lower triangle) and significance (upper triangle) between the variables used in this study. Long: geographical longitude; SST, SSS and SFluor: surface temperature, salinity and fluorescence, respectively; DCM: depth of the chlorophyll maximum; MLD: mixed layer depth; NBSS and NBSI: slope and intercept of the biomass-normalized spectrum, respectively; Tricho, phyto, microz, mesoz, Cope, Tunic, Cnid, and Other: abundance of *Trichodesmium*, phytoplankton, microzooplankton, mesozooplankton, Copepoda, Tunicata, Cnidaria, and other mesozooplankton taxa, respectively. Significant coefficients are indicated in bold.

	Long	SST	SSS	SFluor	DCM	MLD	NBSS	NBSI	Tricho	Phyto	Microz	Mesoz	Cope	Tuni	Cnid	Other
Long		0.000	0.000	0.001	0.303	0.000	0.010	0.003	0.144	0.000	0.000	0.695	0.330	0.205	0.617	0.444
SST	<b>−0.710</b>		0.001	0.000	0.676	0.073	0.005	0.047	0.582	0.005	0.001	0.394	0.127	0.115	0.499	0.469
SSS	<b>0.661</b>	<b>−0.485</b>		0.270	0.001	0.000	0.206	0.001	0.001	0.000	0.001	0.113	0.020	0.060	0.155	0.078
SFluor	<b>0.498</b>	<b>−0.521</b>	0.172		0.033	0.506	0.166	0.625	0.531	0.707	0.321	0.521	0.464	0.364	0.060	0.457
DCM	0.161	0.066	<b>0.491</b>	<b>−0.326</b>		0.000	0.711	0.012	0.009	0.001	0.007	0.146	0.559	0.556	0.020	0.292
MLD	<b>0.559</b>	<b>−0.276</b>	<b>0.585</b>	0.104	<b>0.551</b>		0.043	0.001	0.112	0.001	0.017	0.247	0.314	0.484	0.726	0.432
NBSS	<b>0.393</b>	<b>−0.424</b>	0.199	0.218	0.059	<b>0.314</b>		0.007	0.226	0.031	0.000	0.000	0.215	0.140	0.136	0.230
NBSI	<b>−0.453</b>	<b>0.308</b>	<b>−0.478</b>	<b>−0.078</b>	<b>−0.383</b>	<b>−0.496</b>	<b>−0.413</b>		0.370	0.000	0.000	0.014	0.004	0.004	0.061	0.012
Tricho	0.227	0.086	<b>0.499</b>	<b>−0.098</b>	<b>0.396</b>	0.246	<b>−0.191</b>	<b>−0.142</b>		0.032	0.201	0.067	0.425	0.434	0.012	0.124
phyto	<b>−0.628</b>	<b>0.417</b>	<b>−0.607</b>	<b>−0.059</b>	<b>−0.480</b>	<b>−0.483</b>	<b>−0.333</b>	<b>0.749</b>	<b>−0.328</b>		0.000	0.119	0.009	0.016	0.047	0.031
microz	<b>−0.626</b>	<b>0.474</b>	<b>−0.483</b>	<b>−0.155</b>	<b>−0.403</b>	<b>−0.362</b>	<b>−0.545</b>	<b>0.779</b>	<b>−0.199</b>	<b>0.845</b>		0.999	0.024	0.039	0.090	0.028
mesoz	0.062	<b>−0.133</b>	<b>−0.245</b>	0.101	<b>−0.225</b>	<b>−0.180</b>	<b>0.548</b>	<b>0.377</b>	<b>−0.282</b>	0.241	0.000		0.000	0.000	0.050	0.001
Cope	<b>−0.270</b>	0.412	<b>−0.592</b>	<b>−0.205</b>	<b>−0.164</b>	<b>−0.279</b>	0.340	<b>0.699</b>	<b>−0.223</b>	<b>0.648</b>	<b>0.578</b>	<b>0.892</b>		0.000	0.025	0.000
Tuni	<b>−0.347</b>	0.424	<b>−0.496</b>	<b>−0.253</b>	<b>−0.165</b>	<b>−0.196</b>	0.400	<b>0.690</b>	<b>−0.218</b>	<b>0.609</b>	<b>0.538</b>	<b>0.924</b>	<b>0.928</b>		0.035	0.000
Cnid	0.141	<b>−0.189</b>	<b>−0.386</b>	0.496	<b>−0.593</b>	<b>−0.099</b>	0.403	0.494	<b>−0.630</b>	<b>0.521</b>	0.452	<b>0.514</b>	<b>0.575</b>	<b>0.547</b>		0.005
Other	<b>−0.214</b>	0.203	<b>−0.469</b>	<b>−0.208</b>	<b>−0.291</b>	<b>−0.220</b>	0.330	<b>0.631</b>	<b>−0.415</b>	<b>0.558</b>	<b>0.565</b>	<b>0.756</b>	<b>0.881</b>	<b>0.883</b>	<b>0.684</b>	

The first two components of the PCA on these variables accounted for 78.6% of total variance. Both components were mainly related with plankton variables, while hydrographic variables had generally low influence, with the exception of MLD (Table 4). The first component (PC1, 47.2% of variance) was positively correlated with the abundance of most plankton groups, mainly with mesozooplankton, and negatively correlated with *Trichodesmium*. The second component (PC2, 31.4% of variance) had positive correlations with microzooplankton and phytoplankton and negative correlations with mesozooplankton and *Trichodesmium*. As a result, most of NASE stations resulted with negative values for both components, while those of NASW had generally positive values (Figure 8a). The zonal pattern of these components was different. While PC1 showed a minimum value near the center of the transect (Figure 8b), PC2 increased linearly towards the west (Figure 8c).

**Table 4.** Loadings of the variables on the first two components of the Principal Component Analysis (PCA). SST: sea surface temperature; SSS: sea surface salinity; SFluor: surface chlorophyll fluorescence; DCM: depth of the chlorophyll maximum; MLD: mixed layer depth. Spectral parameters (NBSS, NBSI) and the abundance of *Trichodesmium* and other plankton groups were also included.

Variable	PC 1	PC 2
Longitude	-0.037	-0.139
SST	0.000	0.006
SSS	-0.002	-0.002
SFluor	0.000	0.000
DCM	-0.093	-0.094
MLD	-0.102	-0.122
NBSS	0.000	-0.001
NBSI	0.003	0.003
<i>Trichodesmium</i>	-0.334	-0.174
Phytoplankton	0.312	0.499
Microzooplankton	0.218	0.684
Mesozooplankton	0.851	-0.458

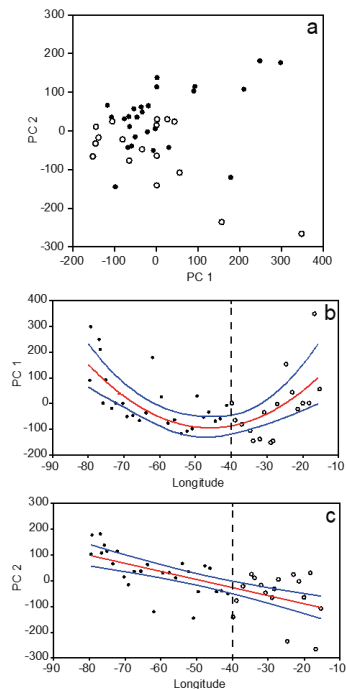


**Figure 8.** Principal Component Analysis (PCA) of all variables considered in this study. (a) Projection of samples in the two first axes (PC 1 and PC 2), and variation with the geographical longitude (degrees, negative to the west) of (b) the scores on the first and (c) second axis. The significant regression line (red) and 95% confidence limits (blue) are indicated. Samples from the Longhurst provinces NASE and NASW are indicated by open and filled dots, respectively. Circles and dots are explained in the caption as “open dots” and “filled dots”, respectively.

## 4. Discussion

We report significant, continuous zonal gradients in hydrographic and plankton variables across the subtropical North Atlantic. Hydrographic gradients were non-linear with maximum or minimum values near the center of the transect. In contrast, most plankton variables showed linear zonal gradients reaching maximum values at one end of the transect. Furthermore, even when total mesozooplankton did not show any significant zonal pattern, its taxonomic composition showed a gradual replacement of large calanoid by small-bodied Cyclopoid copepods from east to west.

### 4.1. Zonal Variability of the North Atlantic Subtropical Gyre

Our results add further confirmation to the spatial heterogeneity of subtropical gyres, formerly considered as relatively homogeneous and predictable [40]. In the particular case of the North Atlantic subtropical gyre, the apparently symmetrical circulation, with surface currents proceeding northwards in the west (the Gulf Stream) and southwards (the Canary Current) in the east, is modulated by intense mesoscale activity in some areas. Cyclones and mesoscale eddies are a common feature in NASW, while they are less frequent and energetic in NASE [40–42]. Such activity has a large influence in pumping nutrients from waters below the pycnocline to the surface layer, thus contributing to a significant fraction of new production in NASW [43]. In contrast, most of the nutrients of NASE are provided by the winter convection [43], but also by upwelling in the Canary Current [44]. In addition, atmospheric nitrogen has been recently identified as a significant input for biological production, not only in NASW [45,46], but also in NASE [19,22,25,29].

Such hydrographic and biogeochemical heterogeneity is consistent with our findings of non-linear gradients. Maximum SST and high variability in the west are expected because the influence of Gulf Stream [4], waters of southern origin in the Florida Strait [47], and eddy activity [40–42]. In turn, maximum salinity near 40° W can be explained by high evaporation rates in this region [23]. A deeper mixed layer at the center of the gyre is expected in the subtropical gyres during winter, as these regions had generally mean annual negative Ekman pumping and are characterized by isothermal layers shallower than the isopycnal ones and a vertical compensation between temperature and salinity [27]. Because the gradients in temperature and salinity, active mixing cannot occur throughout the isopycnal layer, thus limiting the nutrient inputs to diffusion fluxes. This would explain a concomitant increase in the DCM near the center of the gyre and the correlation between MLD and DCM, as observed here and in previous studies [21,24]. In turn, the marked shallowing of the DCM at both ends of the transect corresponds to the fertilizing influence of the upwelling and the Canary Current in the east, and to the Gulf Stream and mesoscale activity in the west [40,42].

In contrast with hydrographic variables, plankton zonal variability could be described mostly by linear gradients. These gradients were not evident in previous studies where latitudinal variability was also recorded [21,24] but reflected the influence of the hydrographical structure and dynamics mostly through the nutrient inputs [40]. The possible cause of this difference between hydrographic and plankton zonal patterns will be addressed in the following section.

### 4.2. Continuous Gradients vs. Discrete Biogeographic Provinces

The division of the ocean in biogeographic biomes and provinces has been useful to summarize biogeochemical fluxes and plankton assemblages in major regions. Particularly, the Longhurst classification [13] is well established among many regional and global studies, including the subtropical Atlantic [21,24,29], as it is based on hydrographic and biological observations. However, other studies revealed several limitations of the use of discrete oceanic zones. For instance, the Longhurst provinces were defined using plankton variables as chlorophyll concentration, primary production, and in situ zooplankton observations, but lacked specific information on phytoplankton assemblages and seasonal succession, and alternative divisions were proposed [14]. Another limitation of the use of fixed regions

is their static nature, as they employ observations integrated through space and time that may not account for internal variability [48,49]. While we also found some correspondence between the zonal distribution of plankton variables and Longhurst provinces NASW and NASE, our approach may help to overcome in part this limitation by providing detailed spatial observations in less explored ocean regions. Alternatively, data for some variables can be obtained by satellite observations at quasi-synoptical time scales over large areas of the ocean, such as for SST, SST and MLD [50], or for surface chlorophyll [48]. Nevertheless, the direct observation of other variables, as zooplankton abundance and composition are still not feasible, and requires a combination of satellite observations of other variables and modelling [51].

Linear zonal gradients in the abundance of phytoplankton, microzooplankton, and *Trichodesmium*, in the parameters of plankton size spectra, and in the composition of zooplankton assemblages, as found in this study, may be the consequence of both hydrographic and biological factors. For instance, water currents redistribute plankton, particularly at both ends of the transect where hydrographic variability is maximal [40,42,44], thus transporting organisms out of the zones where they have grown under environmental conditions that are different from those of their current location. Among the biological factors, species competition and niche packaging may also explain the zonal plankton gradients. Because the abundance of individual plankton species often varies following a Gaussian function, with maximum values at the optimal value of the environmental variable (e.g., temperature), the combination of several species with different optimal values leads to species assemblages that are relatively resilient to environmental variability [52]. For instance, small changes in temperature would have little effect on the abundance of species living near their optimal temperature while causing noticeable decreases in the abundance of species living near their thermal limits. Therefore, gradual changes in environmental conditions would be tolerated by some species but not by others, resulting in changes in abundance for individual species but also for the whole community. In addition, the competition between species increases as they depart from their niche optimal values, where niche separation is maximal, further affecting abundance. In this way, the combination of species with different niches ensures smooth transitions in space and time in the composition and abundance of plankton assemblages despite sudden changes in environmental variability [53]. Modelling studies have shown how plankton communities can self-assemble and adapt to changing environmental conditions under the control by trade-offs related to body size, nutrient acquisition, and sinking [54]. In this way, non-linear gradients in hydrographic variables would be levelled-out by individual species producing linear transitions along the zonal gradient. Mesozooplankton abundance and composition appears somewhat disconnected from gradients in hydrography and other plankton components, but size-fractionated biomass data from the same cruise revealed a non-linear pattern with minimum values near the center of the transect [19]. This can be explained in part by the variation in the individual body size of the dominant organisms (mainly copepods) along the transect, with small bodied species (e.g., *Oithona*) progressively increasing from east to west, as reflected in the second axis for the MDS on the zooplankton taxonomical composition. Thus, increases in small organisms affected more total abundance distribution than biomass distribution. Moreover, the distribution of mesozooplankton biomass in the studied section was closely related with the dominant input of inorganic nitrogen for primary producers: advected nitrogen from deep layers in both ends and atmospheric nitrogen in the central zone, as deduced from stable isotope signatures [19,29], and the presence of *Trichodesmium* and unicellular diazotrophs [22].

Plankton size-spectra, as a summary of plankton composition and function, also showed a gradual transition of assemblages despite the relatively sharp changes in the environment. This is the first study of plankton size spectra along a zonal transect at a fixed latitude in the subtropical North Atlantic, but the results are comparable to those reported in studies following latitudinal gradients. For instance, the decrease in NBSS (i.e., more negative slopes) towards the west indicates the increasing importance of plankton of small

size, as reflected by the accompanying increase in phytoplankton and microzooplankton abundance, and the decrease in *Trichodesmium* filaments. These results are consistent with the described inverse relationship found between NBSS and plankton abundance in a large range of productivity in the Atlantic Ocean [55], while studies focusing only in the central regions found weak or non-significant relationships of the spectral slope with abundance [8,21]. Interestingly, the range of variation of NBSS in this study, computed using carbon biomass, is wider than the range reported for plankton in the North Atlantic, mainly including latitudinal transects between 50° N and 50° S and computed using biovolume (−1.26 to −0.80) [8,21,55,56]. Even when converted to their corresponding biovolume NBSS [56], our values varied between −1.89 and −1.00, extending the range of NBSS for phytoplankton [21,55], but also the values reported in studies also including zooplankton [8,56]. Steeper slopes imply larger energy losses in the transfer from the small and more abundant phytoplankton cells to the larger and less abundant mesozooplankton, and therefore a reduced number of trophic levels [34,57]. Thus, the linear decrease in NBSS (and the corresponding increase in NBSI) from east to west indicates a gradual transition from a food web based on relatively large phytoplankton and mesozooplankton near the Canary Current (flatter slopes) to a food web where small cells and microzooplankton dominate (steeper slopes). The accompanying linear decrease in *Trichodesmium* further enhanced this transition, having a major influence on the transfer of nitrogen up the food web through the transect [19,29].

#### 4.3. Implications for Modelling and Forecasting Subtropical Plankton

While our study did not consider aspects that may be important for a full description of the pelagic ecosystem in subtropical regions, as seasonality [20,24], diel rhythms of plankton [9,24], or the biomass of pico- and nanoplankton [9,21], the results clearly show smooth zonal transitions, rather than sharp boundaries, in the oceanographic conditions and plankton assemblages across biographic provinces. Continuous gradients in plankton variables would facilitate the identification of parallel changes in environmental factors, and may lead to the quantification of causal relationships and empirical functions. For instance, the correlation of zonal trends in phytoplankton and microzooplankton agree with the close coupling of microzooplankton grazing rates with phytoplankton observed in the eastern region of the gyre [9]. In addition, gradients would facilitate model construction and validation (and likely forecasting) by providing smooth transitions between alternative states (e.g., transect endmembers) instead of the traditional approach of modelling changes at discrete regions [15,54]. However, one of the limitations of this approach is that these gradients may exhibit temporal variability, particularly at seasonal and decadal time scales.

Currents and water mass transport in the subtropical North Atlantic have been shown to vary seasonally [58–60], as well as phytoplankton blooms [60,61], although the latter seem to begin earlier and produce less biomass than those of temperate regions. The importance of seasonality in determining the shape of gradients as those found in this study cannot be assessed, as there is only little evidence of zonal variations in seasonality from plankton observations in the subtropical North Atlantic [20,24]. Similarly, interannual and decadal variability was observed in water mass circulation and heat transport [4,23], acidification, and dissolved oxygen [16,17], but almost limited to satellite observations in cases of plankton [5,62]. There is some evidence that warming intensity may affect differently zooplankton biomass in selected areas of NASE [63,64] vs. NASW [65,66]. Therefore, future studies must consider the variability of zonal gradients, as those identified in this study, by including diverse temporal scales. In this way, accounting for temporal and spatial variability would improve the predictions on the effects of global changes on the subtropical North Atlantic, as illustrated by studies of mass transports [4,23,59].

## 5. Conclusions

This study demonstrates the benefits of using empirically constructed continuous gradients versus the use of average values for biogeographical provinces to characterize

plankton assemblages and the main hydrographic constraints in the subtropical north Atlantic. These gradients were non-linear for hydrographic variables but linear for plankton variables, implying a levelling effect of individual species, producing linear transitions along the zonal gradient. The computation of continuous gradients can be further applied to consider the variability related to annual, seasonal, and daily cycles or mesoscale activity.

**Supplementary Materials:** The following supporting information can be downloaded at: <https://www.mdpi.com/article/10.3390/oceans5010007/s1>, Figure S1. Dendrogram of log-transformed mesozooplankton abundance data; Table S1. Correlation between environmental variables; Table S2 Parameters of the 2nd order polynomial relating sea surface temperature, sea surface salinity, mixed layer depth, or the depth of the chlorophyll maximum with geographical longitude.; Table S3. Values of the slope and intercept of the biomass-normalized plankton spectra for each station; Table S4. Values of the linear regression parameters between plankton variables and geographical longitude; Table S5. Abundance (indiv. m<sup>-3</sup>) of mesozooplankton taxa.

**Author Contributions:** Conceptualization, A.B.; methodology, M.Á.L., E.R. and A.F.L.; formal analysis, A.B.; investigation, A.B., M.Á.L. and A.F.L.; data curation, A.B. and M.Á.L.; writing—original draft preparation, A.B.; writing—review and editing, A.B., M.Á.L., E.R. and A.F.L.; visualization, A.B.; project administration, A.B.; funding acquisition, A.B. All authors have read and agreed to the published version of the manuscript.

**Funding:** This research was supported by project Malaspina-2010 (CSD2008-00077) funded by program CONSOLIDER-INGENIO 2010 of the Ministerio de Ciencia e Innovación (Spain).

**Institutional Review Board Statement:** Not applicable.

**Informed Consent Statement:** Not applicable.

**Data Availability Statement:** Hydrographic and nutrient data for this cruise can be found in the database of CLIVAR and CCHDO [27] at <https://cchdo.ucsd.edu/cruise/29AH20110128>, accessed on 1 March 2024. *Trichodesmium* abundance data was incorporated in Version 2 of the global oceanic diazotroph database [11,33] at <https://figshare.com/ndownloader/articles/21677687/versions/3>, accessed on 1 March 2024.

**Acknowledgments:** We are indebted to C.M. Duarte for the successful coordination of the Malaspina 2010 Expedition. We also acknowledge the support of the Chief Scientist of Leg 8, A. Hernández-Guerra, and to the crew and technicians of the R/V Sarmiento de Gamboa for facilitating the collection of samples for this study. Sampling and filtration on board was efficiently made by J. Varela Romay. FlowCAM counts were made by J. Lorenzo and F. Eiroa under the supervision of M. Varela, and mesozooplankton identification was assisted by M.T. Alvarez-Ossorio.

**Conflicts of Interest:** The authors declare no conflicts of interest. The funders had no role in the design of the study; in the collection, analysis, or interpretation of data; in the writing of the manuscript; or in the decision to publish the results.

## References

1. IPCC. Climate Change 2023: Synthesis Report. In *Contribution of Working Groups I, II and III to the Sixth Assessment Report of the Intergovernmental Panel on Climate Change*; IPCC: Geneva, Switzerland, 2023; p. 115.
2. Parrilla, G.; Lavín, A.; Bryden, H.; García, M.; Millard, R. Rising temperatures in the subtropical North Atlantic Ocean over the past 35 years. *Nature* **1994**, *369*, 48–51. [[CrossRef](#)]
3. Lavin, A.M.; Bryden, H.L.; Parrilla, G. Mechanisms of heat, freshwater, oxygen and nutrient transports and budgets at 24.5° N in the subtropical North Atlantic. *Deep Sea Res.* **2003**, *50*, 1099–1128. [[CrossRef](#)]
4. Bryden, H.L.; Longworth, H.R.; Cunningham, S.A. Slowing of the Atlantic meridional overturning circulation at 25° N. *Nature* **2005**, *438*, 655–657. [[CrossRef](#)] [[PubMed](#)]
5. Behrenfeld, M.J.; O'Malley, R.T.; Siegel, D.A.; McClain, C.L.; Sarmiento, J.L.; Feldman, G.C.; Milligan, A.J.; Falkowski, P.G.; Letelier, R.M.; Boss, E.S. Climate-driven trends in contemporary ocean productivity. *Nature* **2006**, *444*, 752–755. [[CrossRef](#)] [[PubMed](#)]
6. Polovina, J.J.; Howell, E.A.; Abecassis, M. Ocean's least productive waters are expanding. *Geophys. Res. Lett.* **2008**, *35*, L03618. [[CrossRef](#)]
7. Signorini, S.R.; Franz, B.A.; McClain, C.R. Chlorophyll variability in the oligotrophic gyres: Mechanisms, seasonality and trends. *Front. Mar. Sci.* **2015**, *2*, 1. [[CrossRef](#)]

8. San Martín, E.; Harris, R.P.; Irigoien, X. Latitudinal variation in plankton size spectra in the Atlantic Ocean. *Deep Sea Res. II* **2006**, *53*, 1560–1572. [[CrossRef](#)]
9. Armengol, L.; Calbet, A.; Franchy, G.; Rodríguez-Santos, A.; Hernández-León, S. Planktonic food web structure and trophic transfer efficiency along a productivity gradient in the tropical and subtropical Atlantic Ocean. *Sci. Rep.* **2019**, *9*, 2044. [[CrossRef](#)]
10. Fernández, A.; Mouriño-Carballido, B.; Bode, A.; Varela, M.; Marañón, E. Latitudinal distribution of *Trichodesmium* spp. and N<sub>2</sub> fixation in the Atlantic Ocean. *Biogeosciences* **2010**, *7*, 3167–3176. [[CrossRef](#)]
11. Shao, Z.; Xu, Y.; Wang, H.; Luo, W.; Wang, L.; Huang, Y.; Agawin, N.S.R.; Ahmed, A.; Benavides, M.; Bentzon-Tilia, M.; et al. Global oceanic diazotroph database version 2 and elevated estimate of global oceanic N<sub>2</sub> fixation. *Earth Syst. Sci. Data* **2023**, *15*, 3673–3709. [[CrossRef](#)]
12. Décima, M. Zooplankton trophic structure and ecosystem productivity. *Mar. Ecol. Prog. Ser.* **2022**, *692*, 23–42. [[CrossRef](#)]
13. Longhurst, A.R. *Ecological Geography of the Sea*, 2nd ed.; Elsevier: Amsterdam, The Netherlands, 2007; p. 542.
14. Hofmann Elizondo, U.; Righetti, D.; Benedetti, F.; Vogt, M. Biome partitioning of the global ocean based on phytoplankton biogeography. *Prog. Oceanogr.* **2021**, *194*, 102530. [[CrossRef](#)]
15. Fernández-Castro, B.; Pahlow, M.; Mouriño-Carballido, B.; Marañón, E.; Oschlies, A. Optimality-based *Trichodesmium* diazotrophy in the North Atlantic subtropical gyre. *J. Plankton Res.* **2016**, *38*, 946–963. [[CrossRef](#)]
16. Pérez, F.F.; Mercier, H.; Vazquez-Rodriguez, M.; Lherminier, P.; Velo, A.; Pardo, P.C.; Roson, G.; Rios, A.F. Atlantic Ocean CO<sub>2</sub> uptake reduced by weakening of the meridional overturning circulation. *Nat. Geosci.* **2013**, *6*, 146–152. [[CrossRef](#)]
17. Guallart, E.F.; Fajar, N.M.; Padín, X.A.; Vázquez-Rodríguez, M.; Calvo, E.; Ríos, A.F.; Hernández-Guerra, A.; Pelejero, C.; Pérez, F.F. Ocean acidification along the 24.5° N section in the subtropical North Atlantic. *Geophys. Res. Lett.* **2015**, *42*, 450–458. [[CrossRef](#)]
18. Marañón, E.; Holligan, P.M.; Varela, M.; Mouriño, B.; Bale, A.J. Basin-scale variability of phytoplankton biomass, production and growth in the Atlantic Ocean. *Deep Sea Res.* **2000**, *47*, 825–857. [[CrossRef](#)]
19. Mompeán, C.; Bode, A.; Benítez-Barrios, V.M.; Domínguez-Yanes, J.F.; Escáñez, J.; Fraile-Nuez, E. Spatial patterns of plankton biomass and stable isotopes reflect the influence of the nitrogen-fixer *Trichodesmium* along the subtropical North Atlantic. *J. Plankton Res.* **2013**, *35*, 513–525. [[CrossRef](#)]
20. Fernández, A.; Marañón, E.; Bode, A. Large-scale meridional and zonal variability in the nitrogen isotopic composition of plankton in the Atlantic Ocean. *J. Plankton Res.* **2014**, *36*, 1060–1073. [[CrossRef](#)]
21. Moreno-Ostos, E.; Blanco, J.M.; Agustí, S.; Lubián, L.M.; Rodríguez, V.; Palomino, R.L.; Llabrés, M.; Rodríguez, J. Phytoplankton biovolume is independent from the slope of the size spectrum in the oligotrophic Atlantic Ocean. *J. Mar. Syst.* **2015**, *152*, 42–50. [[CrossRef](#)]
22. Benavides, M.; Moisaner, P.H.; Daley, M.C.; Bode, A.; Aristegui, J. Longitudinal variability of diazotroph abundances in the subtropical North Atlantic Ocean. *J. Plankton Res.* **2016**, *38*, 662–672. [[CrossRef](#)]
23. Hernández-Guerra, A.; Pelegrí, J.L.; Fraile-Nuez, E.; Benítez-Barrios, V.; Emelianov, M.; Pérez-Hernández, M.D.; Vélez-Belchí, P. Meridional overturning transports at 7.5° N and 24.5° N in the Atlantic Ocean during 1992–1993 and 2010–2011. *Prog. Oceanogr.* **2014**, *128*, 98–114. [[CrossRef](#)]
24. Harrison, W.G.; Aristegui, J.; Head, E.J.H.; Li, W.K.W.; Longhurst, A.R.; Sameoto, D.D. Basin-scale variability in plankton biomass and community metabolism in the sub-tropical North Atlantic Ocean. *Deep Sea Res. II* **2001**, *48*, 2241–2270. [[CrossRef](#)]
25. Fernández, A.; Graña, R.; Mouriño-Carballido, B.; Bode, A.; Varela, M.; Domínguez, J.F.; Escáñez, J.; de Armas, D.; Marañón, E. Community N<sub>2</sub> fixation and *Trichodesmium* spp. abundance along longitudinal gradients in the eastern subtropical North Atlantic. *ICES J. Mar. Sci.* **2013**, *70*, 223–231. [[CrossRef](#)]
26. Grasshoff, K.; Ehrhardt, M.; Kremling, K. *Methods of Seawater Analysis*, 2nd ed.; Verlag Chemie: Weinheim, Germany, 1983; p. 419.
27. de Boyer Montégut, C.; Madec, G.; Fischer, A.S.; Lazar, A.; Iudicone, D. Mixed layer depth over the global ocean: An examination of profile data and a profile-based climatology. *J. Geophys. Res. C Ocean.* **2004**, *109*, C12003. [[CrossRef](#)]
28. Pérez, F.F.; Hernández Guerra, A. CTD Data from Cruise 29AH20110128, Exchange Version. 2015. Available online: <https://cchdo.ucsd.edu/cruise/29AH20110128> (accessed on 1 June 2015).
29. Mompeán, C.; Bode, A.; Gier, E.; McCarthy, M.D. Bulk vs. aminoacid stable N isotope estimations of metabolic status and contributions of nitrogen fixation to size-fractionated zooplankton biomass in the subtropical N Atlantic. *Deep Sea Res.* **2016**, *114*, 137–148. [[CrossRef](#)]
30. Álvarez, E.; Moyano, M.; López-Urrutia, A.; Nogueira, E.; Scharek, R. Routine determination of plankton community composition and size structure: A comparison between FlowCAM and light microscopy. *J. Plankton Res.* **2014**, *36*, 170–184. [[CrossRef](#)]
31. Fluid Imaging Technologies. *FlowCAM@Manual. Version 3.2*; Fluid Imaging Technologies Inc.: Yarmouth, MA, USA, 2012; 162p. Available online: <https://www.fluidimaging.com/> (accessed on 20 June 2014).
32. Bachiller, E.; Fernandes, J.A. Zooplankton image analysis manual: Automated identification by means of scanner and digital camera as imaging devices. *Rev. Investig. Mar.* **2011**, *18*, 17–37.
33. WoRMS Editorial Board. World Register of Marine Species. 2023. Available online: <https://www.marinespecies.org> (accessed on 22 September 2023).
34. Shao, Z.; Xu, Y.; Wang, H.; Luo, W.; Wang, L.; Huang, Y.; Luo, Y.-W. Version 2 of the Global Oceanic Diazotroph Database. 2022. Available online: <https://figshare.com/ndownloader/articles/21677687/versions/3> (accessed on 26 February 2024).
35. Platt, T.; Denman, K. The structure of pelagic marine ecosystems. *Rapp. P.-V. Réun. Cons. Int. Explor. Mer.* **1978**, *173*, 60–65.

36. Blanco, J.M.; Echevarria, F.; Garcia, C.M. Dealing with size spectra: Some conceptual and mathematical problems. *Sci. Mar. (Barc.)* **1994**, *58*, 17–29.
37. Working, H.; Hotelling, H. Applications of the theory of error to the interpretation of trends. *J. Am. Stat. Assoc.* **1929**, *24*, 73–85. [[CrossRef](#)]
38. Magurran, A.E. *Measuring Biological Diversity*; Blackwell Science Ltd.: Oxford, UK, 2004; p. 215.
39. Hammer, Ø.; Harper, D.A.T.; Ryan, P.D. PAST: Paleontological Statistics Software Package for Education and Data Analysis. *Palaeontologia Electronica*. 2001. Available online: [https://palaeo-electronica.org/2001\\_1/past/issue1\\_01.htm](https://palaeo-electronica.org/2001_1/past/issue1_01.htm) (accessed on 6 March 2020).
40. Mouriño-Carballido, B.; Neuer, S.C. Regional differences in the role of eddy pumping in the North Atlantic subtropical gyre. *Oceanography* **2008**, *21*, 52–61. [[CrossRef](#)]
41. Smith, R.D.; Maltrud, M.E.; Bryan, F.O.; Hecht, M.W. Numerical simulation of the North Atlantic Ocean at  $1/10^\circ$ . *J. Phys. Oceanogr.* **2000**, *30*, 1532–1561. [[CrossRef](#)]
42. McGillicuddy, D.J.; Anderson, L.A.; Bates, N.R.; Bibby, T.; Buesseler, K.O.; Carlson, C.A.; Davis, C.S.; Ewart, C.; Falkowski, P.G.; Goldthwait, S.A.; et al. Eddy/wind interactions stimulate extraordinary mid-ocean plankton blooms. *Science* **2007**, *316*, 1021–1026. [[CrossRef](#)]
43. Cianca, A.; Helmke, P.; Mouriño, B.; Rueda, M.J.; Llinás, O.; Neuer, S. Decadal analysis of hydrography and in situ nutrient budgets in the western and eastern North Atlantic subtropical gyre. *J. Geophys. Res. C Ocean.* **2007**, *112*, C07025. [[CrossRef](#)]
44. Pelegrí, J.L.; Aristegui, J.; Cana, L.; González-Dávila, M.; Hernández-Guerra, A.; Hernández-León, S.; Marrero-Díaz, A.; Montero, M.F.; Sangrá, P.; Santana-Casiano, M. Coupling between the open ocean and the coastal upwelling region off northwest Africa: Water recirculation and offshore pumping of organic matter. *J. Mar. Syst.* **2005**, *54*, 3–37. [[CrossRef](#)]
45. Capone, D.G.; Burns, J.A.; Montoya, J.P.; Subramaniam, A.; Mahaffey, C.; Gunderson, T.; Michaels, A.F.; Carpenter, E.J. Nitrogen fixation by *Trichodesmium* spp.: An important source of new nitrogen to the tropical and subtropical North Atlantic Ocean. *Glob. Biogeochem. Cycles* **2005**, *19*, GB2024. [[CrossRef](#)]
46. Olson, E.M.; McGillicuddy, D.J.J.; Dyhrman, S.T.; Waterbury, J.B.; Davis, C.S.; Solow, A.R. The depth-distribution of nitrogen fixation by *Trichodesmium* spp. colonies in the tropical–subtropical North Atlantic. *Deep Sea Res.* **2015**, *104*, 72–91. [[CrossRef](#)]
47. Schmitz Jr, W.J.; Richardson, P.L. On the sources of the Florida Current. *Deep Sea Res.* **1991**, *38*, S379–S409. [[CrossRef](#)]
48. Devred, E.; Sathyendranath, S.; Platt, T. Delineation of ecological provinces using ocean colour radiometry. *Mar. Ecol. Prog. Ser.* **2007**, *346*, 07149. [[CrossRef](#)]
49. Kavanaugh, M.T.; Hales, B.; Saraceno, M.; Spitz, Y.H.; White, A.E.; Letelier, R.M. Hierarchical and dynamic seascapes: A quantitative framework for scaling pelagic biogeochemistry and ecology. *Prog. Oceanogr.* **2014**, *120*, 291–304. [[CrossRef](#)]
50. Foster, D.; Gagne, D.J.; Whitt, D.B. Probabilistic machine learning estimation of ocean mixed layer depth from dense satellite and sparse in situ observations. *J. Adv. Model. Earth Syst.* **2021**, *13*, e2021MS002474. [[CrossRef](#)]
51. Druon, J.-N.; Hèlaouët, P.; Beaugrand, G.; Fromentin, J.-M.; Palialexis, A.; Hoepffner, N. Satellite-based indicator of zooplankton distribution for global monitoring. *Sci. Rep.* **2021**, *9*, 4732. [[CrossRef](#)] [[PubMed](#)]
52. Beaugrand, G. Theoretical basis for predicting climate-induced abrupt shifts in the oceans. *Phil. Trans. R. Soc. B* **2015**, *370*, 20130264. [[CrossRef](#)]
53. Kléparski, L.; Beaugrand, G.; Kirby, R.R. How do plankton species coexist in an apparently unstructured environment? *Biol. Lett.* **2022**, *18*, 20220207. [[CrossRef](#)] [[PubMed](#)]
54. Acevedo-Trejos, E.; Brandt, G.; Bruggeman, J.; Merico, A. Mechanisms shaping size structure and functional diversity of phytoplankton communities in the ocean. *Sci. Rep.* **2015**, *5*, 08918. [[CrossRef](#)] [[PubMed](#)]
55. González-García, C.; Agustí, S.; Aiken, J.; Bertrand, A.; Bittencourt Farias, G.; Bode, A.; Carré, C.; Gonçalves-Araujo, R.; Harbour, D.S.; Huete-Ortega, M.; et al. Basin-scale variability in phytoplankton size-abundance spectra across the Atlantic Ocean. *Prog. Oceanogr.* **2023**, *217*, 103104. [[CrossRef](#)]
56. Quiñones, R.A.; Platt, T.; Rodríguez, J. Patterns of biomass-size spectra from oligotrophic waters of the Northwest Atlantic. *Prog. Oceanogr.* **2003**, *57*, 405–427. [[CrossRef](#)]
57. Zhou, M. What determines the slope of a plankton biomass spectrum? *J. Plankton Res.* **2006**, *28*, 437–448. [[CrossRef](#)]
58. Rayner, D.; Hirschi, J.J.M.; Kanzow, T.; Johns, W.E.; Wright, P.G.; Frajka-Williams, E.; Bryden, H.L.; Meinen, C.S.; Baringer, M.O.; Marotzke, J.; et al. Monitoring the Atlantic meridional overturning circulation. *Deep Sea Res. II* **2011**, *58*, 1744–1753. [[CrossRef](#)]
59. Lozier, M.S. Overturning in the North Atlantic. *Ann. Rev. Mar. Sci.* **2012**, *4*, 291–315. [[CrossRef](#)]
60. Sathyendranath, S.; Longhurst, A.; Caverhill, C.M.; Platt, T. Regionally and seasonally differentiated primary production in the North Atlantic. *Deep Sea Res.* **1995**, *42*, 1773–1802. [[CrossRef](#)]
61. McClain, C.R.; Signorini, S.R.; Christian, J.R. Subtropical gyre variability observed by ocean-color satellites. *Deep Sea Res. II* **2004**, *51*, 281–301. [[CrossRef](#)]
62. Siemer, J.P.; Machín, F.; González-Vega, A.; Arrieta, J.M.; Gutiérrez-Guerra, M.A.; Pérez-Hernández, M.D.; Vélez-Belchí, P.; Hernández-Guerra, A.; Fraile-Nuez, E. Recent trends in SST, Chl-a, productivity and wind stress in upwelling and open ocean areas in the upper Eastern North Atlantic subtropical gyre. *J. Geophys. Res. C Ocean.* **2021**, *126*, e2021JC017268. [[CrossRef](#)]
63. Armengol, L.; Franchy, G.; Ojeda, A.; Hernández-León, S. Plankton community changes from warm to cold winters in the oligotrophic subtropical ocean. *Front. Mar. Sci.* **2020**, *7*, 677. [[CrossRef](#)]

64. Couret, M.; Landeira, J.M.; Santana del Pino, Á.; Hernández-León, S. A 50-year (1971–2021) mesozooplankton biomass data collection in the Canary Current System: Base line, gaps, trends, and future prospect. *Prog. Oceanogr.* **2023**, *216*, 103073. [[CrossRef](#)]
65. Steinberg, D.K.; Lomas, M.W.; Cope, J.S. Long-term increase in mesozooplankton biomass in the Sargasso Sea: Linkage to climate and implications for food web dynamics and biogeochemical cycling. *Glob. Biogeochem. Cycles* **2012**, *26*, GB1004. [[CrossRef](#)]
66. Ivory, J.A.; Steinberg, D.K.; Latour, R.J. Diel, seasonal, and interannual patterns in mesozooplankton abundance in the Sargasso Sea. *ICES J. Mar. Sci.* **2019**, *76*, 217–231. [[CrossRef](#)]

**Disclaimer/Publisher's Note:** The statements, opinions and data contained in all publications are solely those of the individual author(s) and contributor(s) and not of MDPI and/or the editor(s). MDPI and/or the editor(s) disclaim responsibility for any injury to people or property resulting from any ideas, methods, instructions or products referred to in the content.